A Monofunctional and Thermostable Prephenate Dehydratase from the Archaeon *Methanocaldococcus jannaschii*†

Andreas C. Kleeb, Peter Kast, and Donald Hilvert*

Laboratory of Organic Chemistry, ETH Zurich, Hönggerberg HCI F 339, CH-8093 Zurich, Switzerland

Received June 26, 2006; Revised Manuscript Received September 8, 2006

ABSTRACT: Prephenate dehydratase (PDT) is an important but poorly characterized enzyme that is involved in the production of L-phenylalanine. Multiple-sequence alignments and a phylogenetic tree suggest that the PDT family has a common structural fold. On the basis of its sequence, the PDT from the extreme thermophile *Methanocaldococcus jannaschii* (MjPDT) was chosen as a promising representative of this family for pursuing structural and functional studies. The corresponding *pheA* gene was cloned and expressed in *Escherichia coli*. It encodes a monofunctional and thermostable enzyme with an N-terminal catalytic domain and a C-terminal regulatory ACT domain. Biophysical characterization suggests a dimeric (62 kDa) protein with mixed α/β secondary structure elements. MjPDT unfolds in a two-state manner ($T_m = 94$ °C), and its free energy of unfolding [$\Delta G_U(H_2O)$] is 32.0 kcal/mol. The purified enzyme catalyzes the conversion of prephenate to phenylpyruvate according to Michaelis−Menten kinetics ($k_{cat} = 12.3$ s^{-1} and $K_m = 22$ μM at 30 °C), and its activity is pH-independent over the range of pH 5−10. It is feedback-inhibited by L-phenylalanine ($K_i = 0.5$ μM), but not by L-tyrosine or L-tryptophan. Comparison of its activation parameters ($\Delta H^{\ddagger} = 15$ kcal/mol and $\Delta S^{\ddagger} = -3$ cal mol^{-1} K^{-1}) with those for the spontaneous reaction ($\Delta H^{\ddagger} = 17$ kcal/mol and $\Delta S^{\ddagger} = -28$ cal mol^{-1} K^{-1}) suggests that MjPDT functions largely as an entropy trap. By providing a highly preorganized microenvironment for the dehydration−decarboxylation sequence, the enzyme may avoid the extensive solvent reorganization that accompanies formation of the carbocationic intermediate in the uncatalyzed reaction.

Prephenate dehydratases (PDTs)[1] catalyze the conversion of prephenate to phenylpyruvate (Figure 1), the committed step in the biosynthesis of L-phenylalanine in the shikimate pathway (*1*, *2*). In the absence of enzyme, this transformation is acid-catalyzed and proceeds in two steps via a carbocation intermediate (*3*). Kinetic measurements have shown that PDTs accelerate this reaction by a factor of $>10^6$ (*4*, *5*). Although a number of PDTs have been characterized biochemically (*6*−*9*), their structure and mechanism remain poorly understood.

In different organisms, PDTs exist as either monofunctional or multifunctional enzymes. The *Escherichia coli* P-protein, for example, is a bifunctional enzyme that has a PDT domain fused to an AroQ chorismate mutase domain at its N-terminus (*4*). In most cases, PDTs contain a C-terminal regulatory ACT domain which binds L-phenylalanine or other amino acids (*10*). Binding of L-phenylalanine generally has an inhibitory effect, whereas tyrosine often activates the enzyme. Binding of tryptophan, methionine, leucine, isoleucine, and various amino acid derivatives has also been reported (*11*). In an attempt to elucidate important structural and functional features, including residues involved in allosteric regulation, Jensen and co-workers identified nine highly conserved amino acids by aligning 14 PDTs from archaea, bacteria, and yeast (*12*).

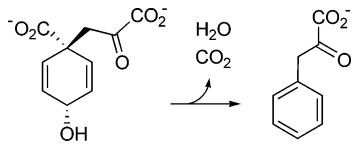

FIGURE 1: Conversion of prephenate to phenylpyruvate.

In this report, we extend the work of Jensen by analyzing multiple-sequence alignments in the Pfam database (*13*) containing all known PDT sequences (currently 393 sequences) from the domains Eucarya, Bacteria, and Archaea. The pattern of residue conservation suggests a common fold for the entire family. From the set of available sequences, we chose the PDT from the archaeon *Methanocaldococcus jannaschii* (MjPDT) as an archetypical monofunctional enzyme for detailed study. Its gene was cloned and expressed, and the encoded protein was biochemically and biophysically characterized. The enzyme is thermostable, highly active, and subject to relatively simple activity regulation. These properties make it a good model system for structural and functional studies.

† This work was supported in part by the ETH Zürich and the Schweizerischer Nationalfonds.

* Corresponding Author. E-mail: hilvert@org.chem.ethz.ch. Phone: +41-44-632-3176. Fax: +41-44-632-1486.

[1] Abbreviations: CD, circular dichroism; CDT, cyclohexadienyl dehydratase; CM, chorismate mutase; ESI, electrospray ionization; GdmCl, guanidinium chloride; IPTG, isopropyl 1-thio-β-D-galactopyranoside; MjPDT, prephenate dehydratase from *Methanocaldococcus jannaschii* (formerly called *Methanococcus jannaschii*); MW, molecular weight; PCR, polymerase chain reaction; PDH, prephenate dehydrogenase; PDT, prephenate dehydratase; SDS, sodium dodecyl sulfate.

10.1021/bi061274n CCC: $33.50
Published on Web 11/02/2006

MATERIALS AND METHODS

Strains and Plasmids. Cloning and protein production were carried out in *E. coli* strain KA13 (*14*, *15*) which lacks chorismate mutase, prephenate dehydrogenase, and prephenate dehydratase and contains an inducible T7 RNA polymerase gene in its genome. The pMG211 plasmid was previously described (*16*).

DNA Manipulations. Molecular cloning was performed according to standard procedures (*17*). Restriction endonucleases and T4 DNA ligase were purchased from New England Biolabs (Ipswich, MA). Oligonucleotides were obtained by custom synthesis from Microsynth (Balgach, Switzerland). Polymerase chain reactions (PCRs) were performed with PfuTurbo polymerase from Stratagene (La Jolla, CA). All segments derived from PCRs in the constructed plasmids were confirmed by DNA sequencing on a 3100-Avant genetic analyzer (Applied Biosystems, Foster City, CA) by chain termination chemistry (*18*), using the BigDye Terminator Cycle Sequencing Kit from the same company.

Plasmid Construction. pAKZ11 was constructed by ligating a PCR fragment containing the *pheA* gene from *M. jannaschii* into appropriately digested pMG211. PCR was performed with the following oligonucleotide primers: MjPDT_N-Term (5′-GGGAATTCCATATGAATAAAG-CAGTTATTTATACATTACCAAAAG) and MjPDT_C-Term (5′-GGACTAGTCATTATTAATCAAAAACTGGG-TATTTTCCTAAAAG). MjPDT_N-Term contains an *Nde*I restriction site (underlined) and a 34-base sequence complementary to the sequence encoding the N-terminus of MjPDT. MjPDT_C-Term contains a 30-base sequence complementary to the sequence encoding the C-terminus of MjPDT, a second TAA stop codon, and a *Spe*I restriction site (underlined). Chromosomal DNA from *M. jannaschii* strain DSM 2661 served as the template. The digested *Nde*I−*Spe*I PCR fragment (831 bp) was ligated to the 4531 bp *Nde*I−*Spe*I fragment of pMG211, yielding pAKZ11 (5356 bp).

Protein Production and Purification. MjPDT was produced in KA13/pAKZ11. LB medium (100 mL) supplemented with 150 μg/mL sodium ampicillin was inoculated with a single colony of KA13/pAKZ11 and incubated overnight at 37 °C. The next day, 4 L of LB medium supplemented with 150 μg/mL sodium ampicillin was inoculated using 80 mL of the overnight culture. The cells were grown at 37 °C to an OD_{600} of 0.6 and then induced by addition of IPTG to a final concentration of 0.2 mM. At the same time, the medium was supplemented with additional ampicillin (30 μg/mL) and the temperature was lowered to 30 °C. After 22 h, the cells were harvested by centrifugation and resuspended in 40 mL of 20 mM Tris-HCl (pH 8.0) supplemented with 1 mg/mL lysozyme and 1 mM Pefabloc SC (Fluka, Buchs, Switzerland). The suspension was kept on ice for 30 min; the cells were sonicated, and the insoluble material was removed by centrifugation (47000*g* for 10 min at 20 °C). The supernatant was incubated at 80 °C for 20 min and centrifuged again (47000*g* for 60 min at 10 °C) to remove heat labile *E. coli* proteins. The supernatant was then dialyzed into 20 mM sodium phosphate buffer (pH 7.0) at room temperature and purified by ion exchange chromatography [low-salt buffer, 20 mM sodium phosphate (pH 7.0); high-salt buffer, 50 mM sodium phosphate (pH 7.2) and 1 M NaCl; MjPDT has a calculated pI of 8.8 using the ProtParam tool on http://www.expasy.org] using a MonoS (HR 10/10) FPLC column from Amersham Pharmacia (Uppsala, Sweden). Active fractions were pooled, concentrated to 3 mL using Makrosep Pall Filters with a 3 kDa cutoff, and then dialyzed into 20 mM Tris-HCl (pH 8.0). Finally, the sample was run over a Superdex 75 HiLoad (26/60) Prep Grade FPLC column from Amersham Pharmacia using 20 mM Tris-HCl (pH 8.0) with 150 mM NaCl as a buffer. The pure protein was concentrated by ultrafiltration (Microsep Pall Filters with a 3 kDa cutoff) to a final concentration of 46 mg/mL as determined by the MicroBC assay (Interchim, Montluçon, France) with bovine serum albumin as a standard. Samples were stored at 4 °C prior to use.

Mass Spectrometry. Proteins were prepared for mass spectrometry by desalting on a NAP-5 column (Amersham Pharmacia) that was preequilibrated with water. Electrospray ionization (ESI) mass spectrometry was carried out on a Finnigan TSQ 7000 mass spectrometer using a mixture of 70% protein solution and 30% acetonitrile.

Analytical Size-Exclusion Chromatography. To analyze the oligomeric state of MjPDT, we performed analytical size-exclusion chromatography on a Superdex 75 (HR 10/30) FPLC column from Amersham Pharmacia. Chromatography was performed at 4 °C using 20 mM Tris-HCl (pH 8.0) containing 150 mM NaCl as a running buffer, a sample volume of 200 mL, and a flow rate of 0.2 mL/min. The elution parameter, K_{av}, was calculated for each protein using the equation $K_{av} = (V_e - V_o)/(V_t - V_o)$, where V_e is the elution volume of the protein. The void volume, V_o, and the total bed volume, V_t, were determined using blue dextran 2000 and acetone, respectively. The following proteins were used for the standard curve: bovine serum albumin (67 kDa), ovalbumin (43 kDa), carbonic anhydrase (29 kDa), ribonuclease A (13.7 kDa), and aprotinin (6.5 kDa). The standards had concentrations of 1−4 mg/mL. MjPDT was injected at concentrations of 0.2−8.0 mg/mL.

Circular Dichroism Spectroscopy. All far-UV circular dichroism (CD) experiments were performed on an Aviv 202 CD spectrometer (Aviv Biomedical, Lakewood, NJ). CD spectra were recorded at 20 °C in 20 mM Tris-HCl (pH 8.0) with a protein concentration of 10 μM and a path length of 0.2 cm. Spectra were obtained by averaging five wavelength scans from 200 to 260 nm in 0.5 nm steps, with a signal averaging time of 2 s and a bandwidth of 1.5 nm. Thermal denaturation curves were determined using 3 μM protein in degassed buffer in a 1.0 cm cuvette with constant stirring. The ellipticity at 218 nm (1.5 nm bandwidth) was measured from 10 to 99 °C in 1 °C steps. For each point, the sample was first equilibrated for 2 min and then the signal was averaged for 1 min before measuring at the next temperature.

Chemical denaturation of MjPDT by guanidinium chloride (GdmCl; BioChemika Ultra from Fluka, >99.5% pure) was monitored by measuring the ellipticity of the sample at 218 nm (1 nm bandwidth). Measurements were made at a final protein concentration of 5 μM in a 0.2 cm quartz cuvette at 25 °C. Each point on the curve was obtained separately by mixing appropriate volumes of buffer [20 mM Tris-HCl (pH 8.0)], MjPDT in buffer, and ~8 M GdmCl in buffer. The samples were allowed to equilibrate at 25 °C for at least 20 min. The ellipticity was then recorded every 1 s for 60 s

and averaged. The averaged value was corrected for the background signal from the buffer (linear interpolation between 0 M GdmCl and the GdmCl stock solution). The accurate concentration of the ~8 M stock solution of GdmCl in 20 mM Tris-HCl (pH 8.0) was calculated from ΔN (the difference between its refractive index and that of PBS) using the equation $[\text{GdmCl}] = 57.147(\Delta N) + 38.68(\Delta N)^2 - 91.60(\Delta N)^3$ (*19*). The free energy of unfolding was calculated by fitting the data to a two-state model as described in reference (*14*).

Analytical Ultracentrifugation. Sedimentation equilibrium experiments were performed on a Beckman XL-A analytical ultracentrifuge equipped with an An-60Ti rotor and two-channel charcoal-Epon cells with quartz windows. Three different protein concentrations (6, 10, and 14 μM) were measured in 20 mM Tris-HCl (pH 8.0) with 150 mM NaCl; 30 μL of FC43 (Sigma-Aldrich, St. Louis, MO) was overlaid with 120 μL of sample, whereas the reference channels contained 160 μL of buffer. One scan per cell was recorded using 0.001 cm point spacing and averaging 20 readings for each point after equilibrium was reached. Sedimentation equilibrium runs were performed at 20 °C using two different rotational speeds, 15 000 and 20 000 rpm. The absorbance was measured at 276 nm. The density of the buffer was measured at 20 °C using a DSA48 density and sound analyzer (Anton Paar, Graz, Austria). The value of V_{bar} was calculated using Sednterp (*20*). Data analysis was performed using Ultrascan (University of Texas Health Science Center, San Antonio, TX).

Coupled Assay for Prephenate Dehydratase Activity. The prephenate dehydratase reaction was assayed by coupling it with the enzyme phenylpyruvate tautomerase (*21*, *22*). Standard solutions of the enol−phenylpyruvate−borate complex were prepared by diluting a fresh 50 mM sodium phenylpyruvate stock solution [dissolved in 20 mM Tris-HCl (pH 8.0)] into 0.5 M boric acid buffer (pH 8.0; adjusted with NaOH) containing 17 μg/mL phenylpyruvate tautomerase from bovine kidney (Sigma-Aldrich). Two equivalents of the tautomerized enol−phenylpyruvate per boron form a stable complex (*23*), which has an absorption maximum at 298 nm. The absorption of the enol−borate complex decreases with an increase in temperature most probably due to a shift in equilibrium. The temperature dependence of the apparent extinction coefficient (ϵ_{app}) at 298 nm was determined by measuring the absorption of the standard solutions (having phenylpyruvate concentrations between 20 and 160 μM) in 10 °C steps from 10 to 90 °C. The solutions were equilibrated at each temperature until the absorption was stable over several minutes. $\Delta\epsilon_{app}$ at any temperature in this range could be estimated from the equation

$$\Delta\epsilon_{app} = -820 + 10600e^{74T} \quad (1)$$

where T is the temperature in degrees Celsius.

Kinetics of the Uncatalyzed Reaction. The rate of the uncatalyzed reaction was determined by monitoring the formation of the enol−phenylpyruvate−borate complex spectrophotometrically at 298 nm. Prephenate solutions were prepared by dissolving barium prephenate (Sigma-Aldrich) in 20 mM Tris-HCl (pH 8.0). The precise concentration of the prephenate stock solution (~7 mM) was obtained by a depletion assay using 2 μM MjPDT to convert prephenate quantitatively to phenylpyruvate, which was detected as the enol−phenylpyruvate−borate complex. For the assay, the prephenate stock solution was diluted in 0.5 M boric acid buffer (pH 8.0) containing 17 μg/mL phenylpyruvate tautomerase to a total volume of 700 μL. Prephenate concentrations from 150 μM to 1 mM were assayed. For each sample, formation of the enol−phenylpyruvate−borate complex was assayed from 40 to 90 °C in 10 °C steps. For each temperature, the samples were preincubated at 40 °C for 10 min before being measured to complex any phenylpyruvate impurities in the prephenate solution. The temperature was then adjusted, and the samples were allowed to equilibrate for an additional 10 min. The change in absorption over time was recorded for 15−60 min. The initial prephenate concentration was derived from the difference between the phenylpyruvate obtained upon full conversion of the added substrate stock solution (using 2 μM MjPDT) and the amount of phenylpyruvate present at the first point of the data set used for velocity determination. The thermodynamic parameters $\Delta H^{\ddagger}$ and $\Delta S^{\ddagger}$ were calculated using the Eyring equation (*24*) and the rate constants for the uncatalyzed reaction (k_{uncat}) determined at different temperatures.

Kinetics of the MjPDT-Catalyzed Reaction. The samples were prepared as they were for the uncatalyzed reaction except for the assays at 10 °C where the samples were allowed to equilibrate for 30 min. The reaction was initiated by adding 0.2−4 nM MjPDT. Initial rates were corrected for the corresponding temperature-specific background reaction (and at 10 and 20 °C for the borate concentration effect)[2] and fitted to the Michaelis−Menten equation to obtain k_{cat} and K_m. The individual k_{cat} values between 10 and 70 °C were used to determine $\Delta H^{\ddagger}$ and $\Delta S^{\ddagger}$ for the MjPDT-catalyzed reaction.

Stop Assay. As a check of the continuous assay, a discontinuous assay of MjPDT was performed at 10, 20, 30, and 70 °C according to the procedure of Gething et al. (*7*). Standards of phenylpyruvate in 1 M NaOH were prepared for all temperatures (the apparent extinction coefficients at 320 nm were $\Delta\epsilon_{10°C} = 17\,600\ M^{-1}\ cm^{-1}$ and $\Delta\epsilon_{70°C} = 10\,300\ M^{-1}\ cm^{-1}$). The reactions were directly performed in thermostated UV cuvettes using 500 μL of 50 mM Tris-HCl (pH 8.0; adjusted at the individual temperatures) and 15 or 3 nM MjPDT at 10 or 20−70 °C, respectively. The reactions were quenched by the addition of 1 volume of 2 M NaOH (carbonate free) which was preincubated at the reaction temperature. The data were fitted to the Michaelis−Menten equation and compared with the results from the continuous assay. The values from the continuous and discontinuous assays differed at most by 10%.[2]

Chorismate Mutase Assay. The CM activity assay was performed by following the method of Sasso et al. (*16*).

[2] Above 30 °C, the k_{cat} and K_m values obtained by the continuous and discontinuous assays differed by ≤10%. Below 30 °C, the coupled assay afforded significantly lower rates (up to 50%) than the stop assay, and the deviation between the two assays increased with a decrease in temperature. Increasing the tautomerase concentration had no measurable effect on the rates, but an inversely proportional dependence of MjPDT activity on the boric acid concentration was observed. By varying the boric acid concentration (between 0.25 and 1 M) and extrapolating to 0 M, we obtained rates for the assays below 30 °C that were within 10% of those seen in the stop assay.

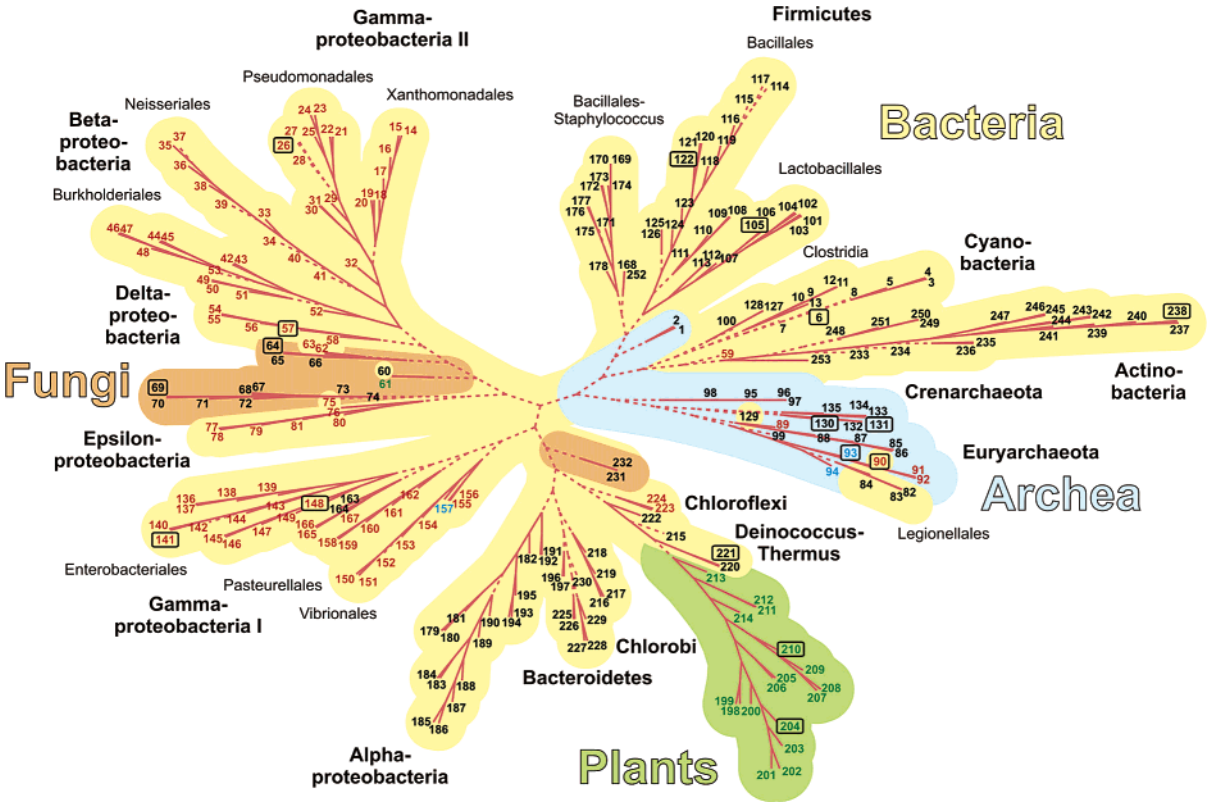

FIGURE 2: Phylogenetic tree of the PDT family. The colored fields correspond to the domains Archaea (blue) and Bacteria (yellow), and the kingdoms Plantae (green) and Fungi (orange). Individual species are numbered (MjPDT is number 131; a complete list can be found in the Supporting Information), and the color of the numbers reflects the domain structure of the enzyme (black for monofunctional, red for bifunctional, blue for trifunctional, and green for enzymes with an appended domain of unknown function). The PDT sequences of the boxed species are aligned in Figure 3. The phylogenetic tree was constructed from a ClustalW alignment using the neighbor-joining method (*39*) with the tools from the webpage provided by the European Bioinformatics Institute (http://www.ebi.ac.uk) and then redrawn in radial form using PhyloDraw (*40*). Additionally, a bootstrap analysis (*41*) was performed to determine the statistical significance of the connections. Connections with bootstrap values of >50% (for 500 iterations) were deemed significant and are drawn as solid lines, whereas the others are rendered as dashed lines.

RESULTS

Sequence Analysis of the PDT Family. PDTs have evolved as monofunctional or multifunctional enzymes with various domain architectures and are often regulated by an appended ACT domain. Currently, 393 PDT sequences from archaea, bacteria, fungi, and plants can be found in the Pfam database (*13*). We have analyzed multiple alignments of the PDT domains of 253 of these sequences (Figure 2; truncated and duplicate sequences were excluded) and compared our results with the work of Jensen and co-workers (*12*), who previously aligned 14 PDT sequences from archaea, bacteria, and yeast. They found nine fully conserved residues in the PDT domain. The only residue that we found to be fully conserved across the entire family is Gly61 (numbered according to the MjPDT sequence). However, with the exception of Asp68 (88% conservation) and Glu81 (91% conservation), all other residues found by Jensen are present in more than 95% of the sequences that were analyzed (Table 1). In addition to these nine residues, we identified a further set of seven residues that are more than 85% conserved (Table 1).

For the purposes of illustration, the conserved residues are highlighted in Figure 3 in an alignment of 17 diverse PDTs. Interestingly, the conservation patterns apply to all domains of life, and the homologies appear to be independent of the flanking protein domain structure. Thus, the phylogenetic tree rendered from the alignments shows that the evolutionary relationship between PDTs does not strictly correlate with their domain architecture (Figure 2).

From the complete set of PDT sequences, we chose the thermostable and monofunctional PDT from *M. jannaschii*, which contains all conserved residues except for Gly9, as a typical representative for detailed structural and functional studies. MjPDT clusters in the phylogenetic tree with PDTs from other archaeal species (Figure 2). The *pheA* gene from *M. jannaschii* strain DSM 2661 encodes a 272-amino acid protein. The Conserved Domain Database (*25*) indicates that the protein consists of an N-terminal PDT domain (residues 1−182) and a C-terminal ACT domain (residues 200−272). The primary sequence of the PDT domain was analyzed using three different algorithms to assess secondary structure content. The enzyme is predicted to be 35% α-helix and 24% *β*-strand (using SSpro), with the secondary structural elements arranged roughly in an alternating fashion (see Figure 4). The predicted secondary structure of the ACT domain agrees with the known three-dimensional structure of the regulatory ACT domain of phosphoglycerate dehydrogenase (*26*).

Cloning, Production, and Purification of MjPDT. pheA was amplified by PCR from *M. jannaschii* chromosomal DNA and ligated into the pMG211 expression vector. MjPDT was produced using the T7 expression system and purified by heat denaturation of the host proteins, followed by ion exchange and size-exclusion chromatography. After

Table 1: Conserved Residues in the PDT Family[a]

amino acids	9[b]	12[b]	18[b]	54[b]	56[b]	57[b]	61[b]	68[b]	81[b]	104[b]	110[b]	145[b]	170[b]	172[b]	173[b]	174[b]
Gly	**99.4**	**88.9**					**100**	0.5				0.4				
Leu	0.6															
Ile					0.5					6.1						
Val			5.0		1.6							4.8				
Ala		8.9	**93.3**	4.4	1.6				4.4			**91.8**	7.1		1.6	
Pro				**95.6**												
Phe								0.5		2.2						**98.4**
Cys												0.4			0.5	
Met		0.6	1.7						0.5	0.6						
Thr						1.6								**99.5**		
Ser						0.5			0.5			2.6		0.5		
Trp																1.6
Tyr		0.6														
Gln								1.6		1.1	**97.3**				0.5	
His								6.6	0.5	**88.4**						
Asn						**97.8**		0.5	0.5				**92.9**			
Asp		0.6						**88.0**	1.6							
Glu					**96.2**			1.1	**91.3**		2.7				0.5	
Lys		0.6						0.5		1.7						
Arg								0.5	0.5						**96.8**	
consensus:	Gly	Gly	Ala	Pro	Glu[c]	Asn[c]	Gly[c]	Asp[c]	Glu[c]	His	Gln[c]	Ala	Asn	Thr[c]	Arg[c]	Phe[c]

[a] Only residues in the PDT domain that are >85% conserved in the 253 analyzed sequences are shown. Conservation is given in percentage, and the amino acids are grouped by their polarity; top to bottom: nonpolar, moderately polar, and very polar (*38*). [b] Residue number in MjPDT. [c] Residues previously identified as being fully conserved (*12*).

purification, 23 mg of pure protein was obtained from 10 g of cells (wet weight) with an overall yield of 6 mg/L of culture. The purity was >98% as judged by SDS−PAGE. The mass of MjPDT obtained by ESI mass spectrometry (31 413 Da) is in good agreement with the calculated mass of 31 415 Da.

Biophysical Characterization. The oligomeric state of MjPDT was examined by size-exclusion chromatography. The protein elutes as an apparent 1.5-mer with a molecular mass of 45.6 kDa, both in the presence and in the absence of 1 mM L-phenylalanine. The nonstoichiometric assembly suggests that the enzyme runs nonideally, presumably because it has a nonspherical shape. In contrast, the data from sedimentation equilibrium experiments fit well to an ideal one-component model with a mass of 61.5 kDa (Figure 5), in good agreement with the calculated dimer mass of 62.8 kDa. The presence of 1 mM L-phenylalanine had no apparent effect on the sedimentation properties.

The far-UV circular dichroism spectrum of MjPDT (Figure 6) shows characteristics of a mixed α/β protein. The α-helical and β-strand contents were estimated by the K2d program (*27*) to be 28 and 24%, respectively, which is in rough agreement with the prediction from the primary sequence (see above). The irreversible unfolding of MjPDT by thermal denaturation was followed by monitoring the change in ellipticity at 218 nm (Figure 7). The midpoint of the unfolding transition (T_m) occurs at 94 °C. In addition, we performed an equilibrium unfolding experiment using GdmCl as a denaturant (MjPDT did not fully unfold in urea at concentrations up to 10 M). A free energy of unfolding [ΔG_U-(H_2O)] of 32.0 ± 1.2 kcal/mol with an m value of −23000 ± 1000 was obtained using a two-state dimer model ($N_2 \rightarrow 2D$) to fit the sigmoidal curve (Figure 8).

Kinetic Measurements. The PDT activity of purified MjPDT follows standard Michaelis−Menten kinetics. At 30 °C, a k_{cat} of 12.3 ± 0.2 s^{-1}, a K_m of 22 ± 1 μM, and a k_{cat}/K_m of 5.6×10^5 M^{-1} s^1 were obtained. In contrast to the rate of the uncatalyzed reaction, which increases linearly with proton concentration (*3*), the enzymatic activity is constant over the range of pH 5−10. At 85 °C, the optimal growth temperature of *M. jannaschii*, k_{cat} is 60-fold higher. Compared to the uncatalyzed conversion of prephenate to phenylpyruvate (Figure 9),[3] MjPDT accelerates the reaction by a factor of 2.8×10^6 at 30 °C and by a factor of 1.9×10^6 at 85 °C. As expected, the enzyme shows no chorismate mutase activity. L-Phenylalanine was found to be an inhibitor with a K_i of 0.5 μM (Figure 10), whereas L-tyrosine and L-tryptophan do not influence MjPDT activity at concentrations up to 1 mM.

The activation parameters for the MjPDT-catalyzed reaction were determined by measuring the temperature dependence of k_{cat} over a wide temperature range (10−70 °C). From the data in Figure 9, an activation enthalpy $\Delta H^{\ddagger}$ of 15 ± 1 kcal/mol and an activation entropy $\Delta S^{\ddagger}$ of −3 ± 3 cal mol^{-1} K^{-1} were obtained. For comparison, $\Delta H^{\ddagger}$ and $\Delta S^{\ddagger}$ for the uncatalyzed reaction are 17 ± 1 kcal/mol and −28 ± 4

[3] Below 40 °C, k_{uncat} agrees well with literature values (*5*). At temperatures above 40 °C, our values are distinctly lower than those previously reported but in good agreement with recently published data obtained by ^{1}H NMR spectroscopy (*36*). The discrepancy can be attributed to the fact that Andrews et al. adjusted the pH of their Tris-HCl buffer at 20 °C, rather than at the temperature of the kinetic measurement (*5*). The prephenate dehydratase reaction is sensitive to pH, and the pH of Tris solutions decreases approximately 0.03 pH units for each 1 °C increase in temperature (*17*).

[4] We assume here that the k_{cat} parameter (largely) reflects the chemical step in catalysis. In response to a suggestion by one of the reviewers, we investigated whether product release might be rate-limiting by running the reaction in the presence of 30% glycerol. Rather than decreasing the rate of reaction, as would be expected if diffusion were limiting, the viscosogen increases enzyme activity somewhat (<2-fold). While the basis of this activation is not entirely clear and assay artifacts cannot yet be entirely ruled out (the additive noticeably interferes with the detection of phenylpyruvate above 50 °C), the activation parameters obtained from the k_{cat} values measured in the presence of the viscosogen in the temperature range of 10−50 °C ($\Delta S^{\ddagger}$ = 4 ± 4 cal mol^{-1} K^{-1} and $\Delta H^{\ddagger}$ = 17 ± 1 kcal/mol) support the general conclusion that MjPDT functions as an entropy trap.

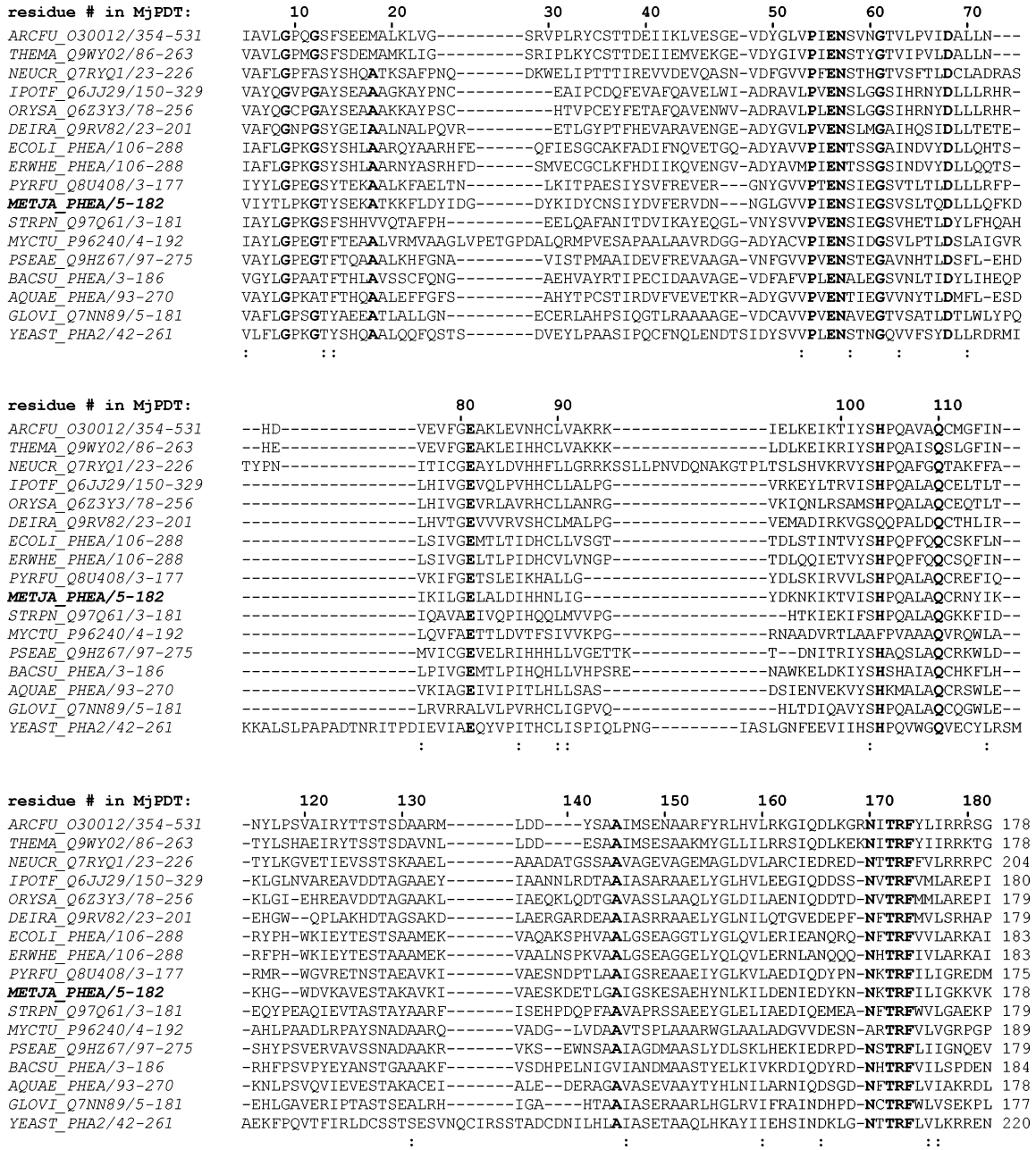

FIGURE 3: Alignment of the prephenate dehydratase domains of 17 PDTs from all domains of life. The >85% conserved residues (highlighted in bold) are numbered according to the MjPDT sequence. Less conserved positions are marked with a colon. Organisms are listed by abbreviation, taxonomy, modular organization, and number in the phylogenetic tree of Figure 2: ARCFU, *Archaeoglobus fulgidus* (Archaea, trifunctional, 93); THEMA, *Thermotoga maritima* (Bacteria, bifunctional, 90); NEUCR, *Neurospora crassa* (Fungi, monofunctional, 64); IPOTF, *Ipomoea trifida* (Plantae, enzyme with an appended domain of unknown function, 204); ORYSA, *Oryza sativa* (Plantae, enzyme with an appended domain of unknown function, 210); DEIRA, *Deinococcus radiodurans* (Bacteria, monofunctional, 221); ECOLI, *E. coli* (Bacteria, bifunctional, 141); ERWHE, *Erwinia herbicola* (Bacteria, bifunctional, 148); PYRFU, *Pyrococcus furiosus* (Archaea, monofunctional, 130); METJA, *M. jannaschii* (Archaea, monofunctional, 131); STRPN, *Streptococcus pneumoniae* (Bacteria, monofunctional, 105); MYCTU, *Mycobacterium tuberculosis* (Bacteria, monofunctional, 238); PSEAE, *Pseudomonas aeruginosa* (Bacteria, bifunctional, 26); BACSU, *Bacillus subtilis* (Bacteria, monofunctional, 122); AQUAE, *Aquifex aeolicus* (Bacteria, bifunctional, #57); GLOVI, *Gloeobacter violaceus* (Bacteria, monofunctional, 6); YEAST, *Saccharomyces cerevisiae* (Fungi, monofunctional, 69).

cal mol^{-1} K^{-1}, respectively. Apparently, the 9 kcal/mol reduction in free energy of activation accomplished by MjPDT at 30 °C is achieved largely by lowering the entropy barrier for reaction.[4]

DISCUSSION

The conversion of prephenate to phenylpyruvate is the penultimate step in the biosynthesis of the essential aromatic amino acid L-phenylalanine. In nature, at least two distinct classes of enzymes, cyclohexadienyl dehydratases (CDTs) and prephenate dehydratases (PDTs), have evolved to catalyze this transformation. CDTs, which share no sequence homology with PDTs,[5] additionally convert arogenate, which is obtained by transamination of prephenate, directly to phenylalanine. While relatively few CDTs have been annotated to date, numerous PDTs have been identified and are abundant in all domains of life. However, despite their role in a key metabolic pathway and the importance of PDT in the commercial production of phenylalanine (*28*), neither the structure nor the mechanism of action of either enzyme

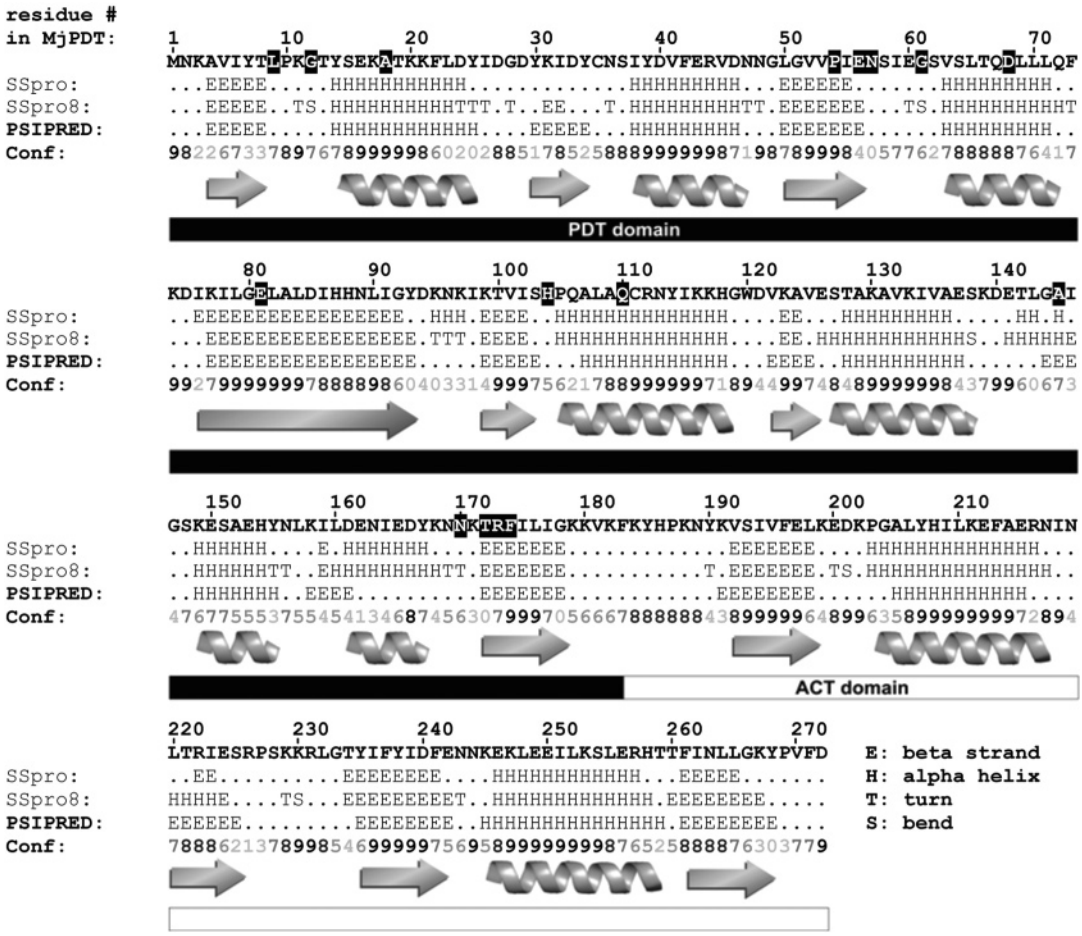

FIGURE 4: Secondary structure prediction of MjPDT from two different prediction servers. SSpro and SSpro8 are predictions from the SCRATCH server (*42*) (http://www.igb.uci.edu/servers/psss.html). PSIPRED (http://bioinf.cs.ucl.ac.uk/psipred) (*43*) additionally provides a confidence value (0 = low, 9 = high). The predicted secondary structure of the appended ACT domain agrees well with that observed in phosphoglycerate dehydrogenase (*26*). Conserved residues are highlighted in black.

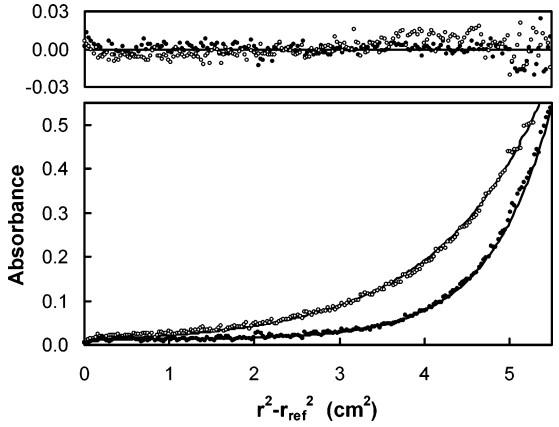

FIGURE 5: Investigation of the MjPDT quaternary structure by analytical ultracentrifugation. Representative sedimentation equilibrium data for MjPDT were obtained with a 14 μM sample at 15 000 (○) and 20 000 rpm (●). The residuals for the fit to an ideal one-component model (solid line) are shown at the top.

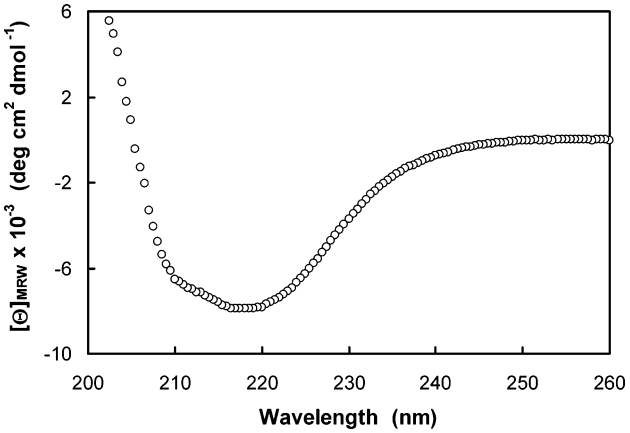

FIGURE 6: Far-UV circular dichroism (CD) spectrum of MjPDT in 20 mM Tris-HCl (pH 8.0) at 20 °C. $[\Theta]_{MRW}$ is the mean molar ellipticity per residue.

class has been definitively elucidated.

Our phylogenetic analysis confirms that PDTs constitute a highly conserved family of enzymes. Although individual PDTs are often components of large, multifunctional proteins, sequence similarity among them appears to be independent of their greater molecular context. The PDT domain, which is predicted to have a mixed α/β secondary structure in accord with our experimental CD data, presumably arose once and was subsequently fused to other functional units—including chorismate mutases, prephenate dehydrogenases, and regulatory domains—as needed to allow coordinated expression or more effective regulation of these various activities in different hosts. The monofunctional PDT from *M. jannaschii*, which clusters with proteins from other archaeal species, is archetypal. It is highly thermostable (T_m = 94 °C) and promotes the decomposition of prephenate with a $>10^6$-fold rate acceleration over a wide range of

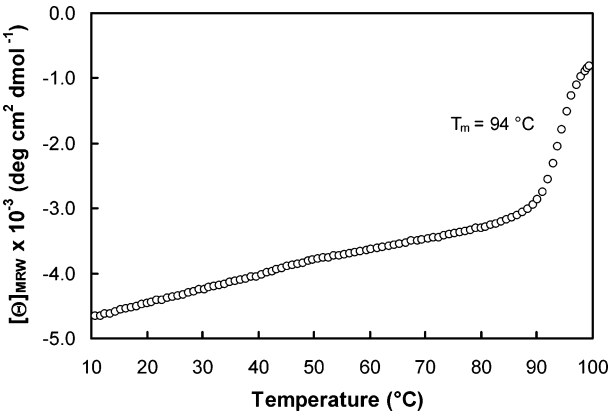

FIGURE 7: Temperature-dependent unfolding of MjPDT determined by CD spectroscopy at 218 nm. The midpoint of the unfolding transition, T_m, was obtained by a Boltzmann sigmoidal curve fit between 88 and 99 °C.

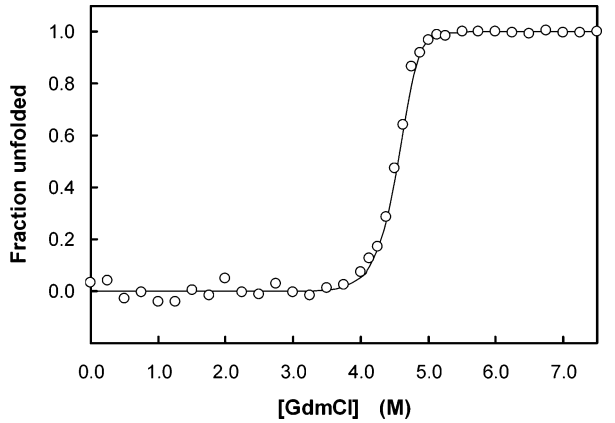

FIGURE 8: Guanidinium chloride-induced denaturation of MjPDT at 25 °C. The fraction of unfolded protein was determined by CD spectroscopy at 218 nm. The curve was fitted to a two-state model (*14*) with a transition midpoint at 4.54 M GdmCl.

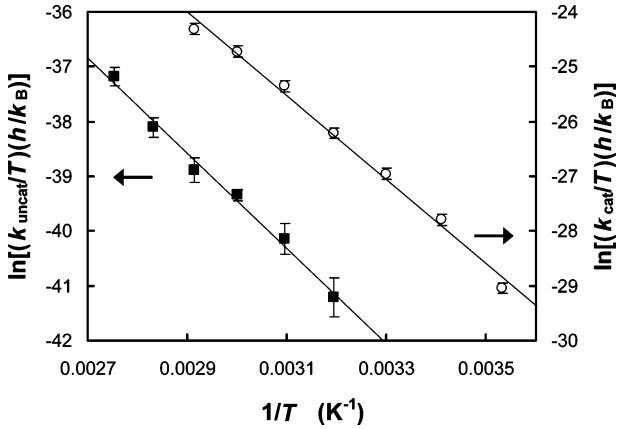

FIGURE 9: Temperature dependence of k_{cat} (○) and k_{uncat} (■) for the transformation of prephenate to phenylpyruvate.

temperatures. Its catalytic domain, spanning residues 1−182, is fused only to a C-terminal ACT domain. On the basis of the properties of proteins containing the latter domain (*26*) and mutagenesis studies of *E. coli* PheA (the P-protein) (*4*), the ACT module is probably responsible for both dimerization of MjPDT and its inhibition by phenylalanine.

Fifteen of the 16 residues that are highly conserved across the entire PDT family are found in MjPDT. Replacement of

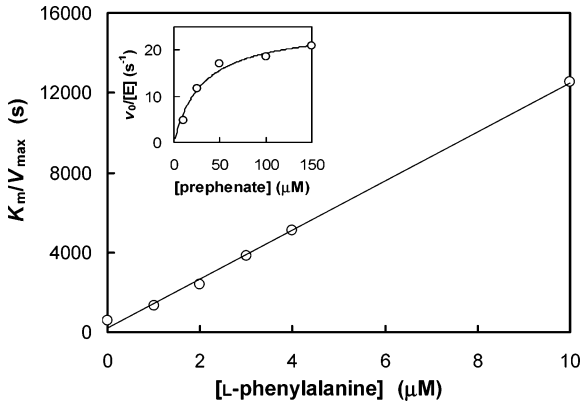

FIGURE 10: Inhibition of MjPDT by L-phenylalanine. The K_i value is obtained by plotting K_m/V_{max} from the individually fitted Michaelis−Menten curves against the L-phenylalanine concentration. The slope in this plot equals $K_m/(V_{max}K_i)$. The inset shows a typical Michaelis−Menten curve obtained in the absence of L-phenylalanine.

Gly9 with leucine represents the only deviation from this consensus. Although detailed functional assignments of these residues are not possible in the absence of high-resolution structural data, the conserved glycines (Gly12 and Gly61) are most likely structural determinants, as they occur in predicted turn regions (Figure 4). The four hydrophobic residues (Ala18, Pro54, Ala145, and Phe174) may similarly help define the fold of the PDT domain, or they may constitute apolar regions of the active site. Because prephenate is a highly polar molecule, with two negatively charged carboxylates, a ketone, and an alcohol moiety, the strongly conserved polar residues in the enzyme are most likely involved in substrate recognition and catalysis. Nevertheless, the presence of only a single positively charged residue in this set, Arg173, suggests that ligand recognition in PDTs is fundamentally different from that in chorismate mutases, which also bind prephenate but have active sites that are rich in cationic residues (*29*−*31*). The recently determined active site of prephenate dehydrogenase from *Aquifex aeolicus* (*32*), which catalyzes the oxidative decarboxylation of prephenate to give 4-hydroxyphenylpyruvate, may prove to be a better analogy for the MjPDT active site. Its binding pocket is lined predominantly with neutral polar residues, including a histidine that is believed to hydrogen bond with the C4 hydroxyl group of prephenate. The substrate carboxylates probably bind near two cationic residues, an arginine and a lysine, although the presence of a nearby aspartate and glutamate preserves the net neutrality of the active site. Similar hydrogen bonding interactions between prephenate and PDT could conceivably be exploited to facilitate departure of water, whereas desolvation of the ring carboxylate upon partitioning from aqueous solution would promote decarboxylation.

Our observation that the MjPDT reaction is essentially pH independent in the range of 5−10 supports the involvement of a weak acid in the elimination of water or, alternatively,

[5] We aligned the 26 sequences annotated as CDTs in the sequence database and compared them with the PDT sequences shown in Figure 3. In agreement with an earlier analysis by Jensen and co-workers (*37*), we found no significant overall similarities. In particular, there was no correspondence of the highly conserved residues in CDTs and PDTs (analysis not shown).

stabilization of the departing hydroxide ion by hydrogen bonding. Consistent with an absence of specific catalytic residues that might participate directly in the reaction, the PDT active site is known to be rather resilient to mutation. In a previous mutagenesis study of 15 polar residues in the *E. coli* P-protein, only four residues, corresponding to Asn57, Ser103, Gln110, and Thr172 in MjPDT, were found to impair activity significantly when mutated to alanine (*6*). Notably, none of the glutamates or aspartates in the protein, which might have served as general acids to assist in the elimination of water, was found to be essential for catalysis. Replacement of the conserved histidine likewise resulted in a mere 10-fold decrease in specific activity.

The observation that MjPDT functions primarily as an entropy trap[4] nevertheless implies that the enzyme-catalyzed reaction takes place in a highly preorganized microenvironment. The uncatalyzed reaction occurs via a two-step mechanism, involving initial protonation and elimination of water to afford a carbocationic intermediate that subsequently undergoes decarboxylation (*3*). The formation of such a charged species entails recruitment of a proton from solution and substantial ordering of solvent water molecules, processes that can give rise to entropies of activation in the range of -10 to -30 cal mol^{-1} K^{-1} (*33*, *34*), in good agreement with the large entropic barrier observed for the thermal conversion of prephenate to phenylpyruvate ($\Delta S^{\ddagger} = -28$ cal mol^{-1} K^{-1}). In providing a preorganized reaction chamber that facilitates the elimination of water and simultaneously stabilizes the high-energy cationic intermediate, the enzyme would eliminate the need for extensive solvent reorganization as the reaction proceeds, thereby reducing the entropic barrier substantially as observed experimentally ($\Delta\Delta S^{\ddagger} \approx 25$ cal mol^{-1} K^{-1}). At the extreme, the enzyme may even favor a mechanism more concerted than that accessible in solution, with decarboxylation occurring simultaneously with dehydration, as has been proposed for the oxidative decarboxylation catalyzed by prephenate dehydrogenase (*3*).

Although MjPDT is a highly efficient enzyme, with k_{cat}/K_m values within 2−3 orders of magnitude of the diffusion limit, prephenate is an intrinsically unstable molecule. Its half-life at 85 °C is approximately 34 min at pH 8 (as estimated from the data in Figure 9) and substantially shorter at lower pH values. Given this, why does *M. jannaschii* require an enzyme for the production of phenylpyruvate? Minimization of problems associated with the decomposition of prephenate to epi-prephenate and other undesired side products is likely to be one reason (*3*). Catalysis also guarantees proper partitioning of prephenate toward phenylalanine rather than tyrosine. The spontaneous decomposition of prephenate to phenylpyruvate is too slow to compete with the enzymatic conversion of prephenate to 4-hydroxyphenylpyruvate, which is an essential step in tyrosine biosynthesis but does not occur without enzymatic assistance. Finally, unlike many thermostable enzymes, MjPDT is active over a wide temperature range. In fact, because of its relatively low K_m value, the apparent second-order rate constant at 37 °C can be estimated to be 1.2×10^6 M^{-1} s^{-1} (Figure 9), which is ca. 20-fold higher than the value reported for *E. coli* PheA under the same conditions (*6*). As a consequence, *M. jannaschii* has the flexibility to survive at lower temperatures where the spontaneous reaction of prephenate is less efficient (*35*).

In summary, MjPDT is a prototype of a highly conserved family of catalysts in the shikimate pathway. It exhibits high stability, high catalytic efficiency, and a simple mechanism of regulation. The absence of unrelated functions makes this protein an attractive starting point for more detailed structural and functional investigations.

ACKNOWLEDGMENT

We thank Sophie Maisnier-Patin for providing chromosomal DNA from *M. jannaschii*, Joris Beld for performing and analyzing the analytical ultracentrifugation experiments, and Kenneth Woycechowsky for helpful discussions.

SUPPORTING INFORMATION AVAILABLE

List of aligned prephenate dehydratases from diverse organisms displayed in the phylogenetic tree in Figure 2. This material is available free of charge via the Internet at http://pubs.acs.org.

REFERENCES

1. Knaggs, A. R. (2001) The biosynthesis of shikimate metabolites, *Nat. Prod. Rep. 18*, 334−355.
2. Haslam, E. (1993) *Shikimic acid: Metabolism and metabolites*, Wiley, New York.
3. Hermes, J. D., Tipton, P. A., Fisher, M. A., O'Leary, M. H., Morrison, J. F., and Cleland, W. W. (1984) Mechanisms of enzymatic and acid-catalyzed decarboxylations of prephenate, *Biochemistry 23*, 6263−6275.
4. Zhang, S., Pohnert, G., Kongsaeree, P., Wilson, D. B., Clardy, J., and Ganem, B. (1998) Chorismate mutase-prephenate dehydratase from *Escherichia coli*: Study of catalytic and regulatory domains using genetically engineered proteins, *J. Biol. Chem. 273*, 6248−6253.
5. Andrews, P. R., Smith, G. D., and Young, I. G. (1973) Transition-state stabilization and enzymic catalysis: Kinetic and molecular orbital studies of rearrangement of chorismate to prephenate, *Biochemistry 12*, 3492−3498.
6. Zhang, S., Wilson, D. B., and Ganem, B. (2000) Probing the catalytic mechanism of prephenate dehydratase by site-directed mutagenesis of the *Escherichia coli* P-protein dehydratase domain, *Biochemistry 39*, 4722−4728.
7. Gething, M.-J. H., Davidson, B. E., and Dopheide, T. A. A. (1976) Chorismate mutase/prephenate dehydratase from *Escherichia coli* K12. 1. The effect of NaCl and its use in a new purification involving affinity chromatography on sepharosyl-phenylalanine, *Eur. J. Biochem. 71*, 317−325.
8. Fischer, R., and Jensen, R. A. (1987) Prephenate dehydratase (monofunctional), *Methods Enzymol. 142*, 507−512.
9. Davidson, B. E. (1987) Chorismate mutase-prephenate dehydratase from *Escherichia coli*, *Methods Enzymol. 142*, 432−439.
10. Aravind, L., and Koonin, E. V. (1999) Gleaning non-trivial structural, functional and evolutionary information about proteins by iterative database searches, *J. Mol. Biol. 287*, 1023−1040.
11. Pierson, D. L., and Jensen, R. A. (1974) Metabolic interlock: Control of an interconvertible prephenate dehydratase by hydrophobic amino acids in *Bacillus subtilis*, *J. Mol. Biol. 90*, 563−579.
12. Gu, W., Williams, D. S., Aldrich, H. C., Xie, G., Gabriel, D. W., and Jensen, R. A. (1997) The AroQ and PheA domains of the bifunctional P-protein from *Xanthomonas campestris* in a context of genomic comparison, *Microb. Comp. Genomics 2*, 141−158.
13. Bateman, A., Coin, L., Durbin, R., Finn, R. D., Hollich, V., Griffiths-Jones, S., Khanna, A., Marshall, M., Moxon, S., Sonnhammer, E. L. L., Studholme, D. J., Yeats, C., and Eddy, S. R. (2004) The Pfam protein families database, *Nucleic Acids Res. 32*, D138−D141.
14. MacBeath, G., Kast, P., and Hilvert, D. (1998) A small, thermostable, and monofunctional chorismate mutase from the archeon *Methanococcus jannaschii*, *Biochemistry 37*, 10062−10073.
15. MacBeath, G., and Kast, P. (1998) UGA read-through artifacts−When popular gene expression systems need a pATCH, *BioTechniques 24*, 789−794.

16. Sasso, S., Ramakrishnan, C., Gamper, M., Hilvert, D., and Kast, P. (2005) Characterization of the secreted chorismate mutase from the pathogen *Mycobacterium tuberculosis*, *FEBS J. 272*, 375−389.
17. Sambrook, J., Fritsch, E. F., and Maniatis, T. (1989) *Molecular cloning: A laboratory manual*, 2nd ed., Cold Spring Harbor Laboratory Press, Plainview, NY.
18. Sanger, F., Nicklen, S., and Coulson, A. R. (1977) DNA sequencing with chain-terminating inhibitors, *Proc. Natl. Acad. Sci. U.S.A. 74*, 5463−5467.
19. Nozaki, Y. (1972) The preparation of guanidine hydrochloride, *Methods Enzymol. 26*, 43−50.
20. Laue, T. M., Shah, B. D., Ridgeway, T. M., and Pelletier, S. L. (1992) *Computer-aided interpretation of analytical sedimentation data for proteins*, Royal Society of Chemistry, Cambridge, U.K.
21. Blasi, F., Fragomel, F., and Covelli, I. (1969) Thyroidal phenylpyruvate tautomerase, *J. Biol. Chem. 244*, 4864−4870.
22. Pirrung, M. C., Chen, J., Rowley, E. G., and McPhail, A. T. (1993) Mechanistic and stereochemical study of phenylpyruvate tautomerase, *J. Am. Chem. Soc. 115*, 7103−7110.
23. Knox, W. E., and Pitt, B. M. (1957) Enzymic catalysis of the keto-enol tautomerization of phenylpyruvic acids, *J. Biol. Chem. 225*, 675−688.
24. Wynne-Jones, W. F. K., and Eyring, H. (1935) The absolute rate of reactions in condensed phases, *J. Chem. Phys. 3*, 492−502.
25. Marchler-Bauer, A., Anderson, J. B., Cherukuri, P. F., DeWeese-Scott, C., Geer, L. Y., Gwadz, M., He, S. Q., Hurwitz, D. I., Jackson, J. D., Ke, Z., Lanczycki, C. J., Liebert, C. A., Liu, C. L., Lu, F., Marchler, G. H., Mullokandov, M., Shoemaker, B. A., Simonyan, V., Song, J. S., Thiessen, P. A., Yamashita, R. A., Yin, J. J., Zhang, D. C., and Bryant, S. H. (2005) CDD: A conserved domain database for protein classification, *Nucleic Acids Res. 33*, D192−D196.
26. Schuller, D. J., Grant, G. A., and Banaszak, L. J. (1995) The allosteric ligand site in the V_{max}-type cooperative enzyme phosphoglycerate dehydrogenase, *Nat. Struct. Biol. 2*, 69−76.
27. Andrade, M. A., Chacon, P., Merelo, J. J., and Moran, F. (1993) Evaluation of secondary structure of proteins from UV circular-dichroism spectra using an unsupervised learning neural-network, *Protein Eng. 6*, 383−390.
28. Grinter, N. J. (1998) Developing an L-phenylalanine process, *CHEMTECH 28*, 33−37.
29. Chook, Y. M., Gray, J. V., Ke, H., and Lipscomb, W. N. (1994) The monofunctional chorismate mutase from *Bacillus subtilis*. Structure determination of chorismate mutase and its complexes with a transition state analog and prephenate, and implications for the mechanism of the enzymatic reaction, *J. Mol. Biol. 240*, 476−500.
30. Lee, A. Y., Karplus, P. A., Ganem, B., and Clardy, J. (1995) Atomic structure of the buried catalytic pocket of *Escherichia coli* chorismate mutase, *J. Am. Chem. Soc. 117*, 3627−3628.
31. Sträter, N., Schnappauf, G., Braus, G., and Lipscomb, W. N. (1997) Mechanisms of catalysis and allosteric regulation of yeast chorismate mutase from crystal structures, *Structure 5*, 1437−1452.
32. Sun, W., Singh, S., Zhang, R., Turnbull, J. L., and Christendat, D. (2006) Crystal structure of prephenate dehydrogenase from *Aquifex aeolicus*: Insights into the catalytic mechanism, *J. Biol. Chem. 281*, 12919−12928.
33. Schaleger, L. L., and Long, F. A. (1963) Entropies of activation and mechanisms of reactions in solution, *Adv. Phys. Org. Chem. 1*, 1−33.
34. Robertson, R. E. (1967) Solvolysis in water, *Prog. Phys. Org. Chem. 4*, 213−280.
35. Bult, C. J., White, O., Olsen, G. J., Zhou, L. X., Fleischmann, R. D., Sutton, G. G., Blake, J. A., FitzGerald, L. M., Clayton, R. A., Gocayne, J. D., Kerlavage, A. R., Dougherty, B. A., Tomb, J. F., Adams, M. D., Reich, C. I., Overbeek, R., Kirkness, E. F., Weinstock, K. G., Merrick, J. M., Glodek, A., Scott, J. L., Geoghagen, N. S. M., Weidman, J. F., Fuhrmann, J. L., Nguyen, D., Utterback, T. R., Kelley, J. M., Peterson, J. D., Sadow, P. W., Hanna, M. C., Cotton, M. D., Roberts, K. M., Hurst, M. A., Kaine, B. P., Borodovsky, M., Klenk, H. P., Fraser, C. M., Smith, H. O., Woese, C. R., and Venter, J. C. (1996) Complete genome sequence of the methanogenic archaeon, *Methanococcus jannaschii*, *Science 273*, 1058−1073.
36. Wright, S. K., DeClue, M. S., Mandal, A., Lee, L., Wiest, O., Cleland, W. W., and Hilvert, D. (2005) Isotope effects on the enzymatic and nonenzymatic reactions of chorismate, *J. Am. Chem. Soc. 127*, 12957−12964.
37. Zhao, G., Xia, T., Fischer, R. S., and Jensen, R. A. (1992) Cyclohexadienyl dehydratase from *Pseudomonas aeruginosa*: Molecular cloning of the gene and characterization of the gene product, *J. Biol. Chem. 267*, 2487−2493.
38. Wolfenden, R., Andersson, L., Cullis, P. M., and Southgate, C. C. B. (1981) Affinities of amino acid side chains for solvent water, *Biochemistry 20*, 849−855.
39. Saitou, N., and Nei, M. (1987) The neighbor-joining method: A new method for reconstructing phylogenetic trees, *Mol. Biol. Evol. 4*, 406−425.
40. Choi, J. H., Jung, H. Y., Kim, H. S., and Cho, H. G. (2000) PhyloDraw: A phylogenetic tree drawing system, *Bioinformatics 16*, 1056−1058.
41. Felsenstein, J. (1985) Confidence limits on phylogenies: An approach using the bootstrap, *Evolution 39*, 783−791.
42. Pollastri, G., Przybylski, D., Rost, B., and Baldi, P. (2002) Improving the prediction of protein secondary structure in three and eight classes using recurrent neural networks and profiles, *Proteins: Struct., Funct., Genet. 47*, 228−235.
43. McGuffin, L. J., Bryson, K., and Jones, D. T. (2000) The PSIPRED protein structure prediction server, *Bioinformatics 16*, 404−405.

BI061274N